Blucher Mechanical Engineering Proceedings
May 2014, vol. 1 , num. 1
www.proceedings.blucher.com.br/evento/10wccm

10th World Congress on Computational Mechanics
8-13 July 2012 • São Paulo • Brazil

A Molecular Dynamics derived Finite Element Method for Structural Simulations and Failure of Graphene Nanocomposites

A. A. R. Wilmes [1], S. T. Pinho[2]

[1] Department of Aeronautics, Imperial College London (andre.wilmes07@imperial.ac.uk)

[2] Department of Aeronautics, Imperial College London (silvestre.pinho@imperial.ac.uk)

Abstract. *The recent rise of 2D materials, such as graphene, has expanded the interest in nano-electromechanical systems (NEMS). The increasing ability of synthesizing more exotic NEMS architectures, creates a growing need for a cost-effective, yet accurate nano-scale simulation method. Established methodologies like Molecular Dynamics (MD) trail behind synthesis capabilities because the computational effort scales quadratically. The equilibrium equations of MD are equivalent with those of the computationally more favourable Finite Element Method (FEM). However, current implementations exploiting this equivalence remain limited due to the FEM iterative solvers requiring a large number of lengthy force field derivatives and specifically tailored element topologies. This paper proposes a formal derivation of the merged Molecular Dynamic Finite Element Method (MDFEM) which establishes an uncoupling of the force field potentials from the element topologies. An implementation approach, which does not require manual derivations, is presented. Different non-linear MD force field potentials are implemented exactly within the FEM, at reduced computational costs. The proposed multi-scale and multi-physics compatible MDFEM is equivalent to to the MD as demonstrated by an example of brittle fracture in Carbon Nanotubes (CNT).*

Keywords: *MDFEM, FEM, AFEM, Molecular, Fracture.*

1. INTRODUCTION

Simulating the mechanical response of nano-structures is important for a wide and rapidly increasing range of areas. Continuous progress in nano-synthesis capabilities, together with graphene's first applications in nano-electromechanical systems (NEMS) [1–3], have further spurred interest in efficient, robust and flexible numerical nano-simulation methods.

One of the main challenges for nano-simulation models consists of achieving a suitable balance between the accuracy of the physical representation and the scale of applicability. At one extreme, *Ab Initio* simulations, based on Density Functional Theory (DFT), can offer high accuracy but cannot readily be used for domains beyond $\mathcal{O}(10^2)$ atoms. At the other extreme, classical Molecular Mechanics (MM) and Dynamics (MD) methods [4–6] only resolve nuclei motion (Born-Oppenheimer approximation), but may be typically applied to domains with

$\mathcal{O}(10^9)$ atoms [7]. Parallel supercomputing simulations have succeeded in increasing this number to $\mathcal{O}(10^{12})$ atoms [8]. A variety of intermediate theory levels have emerged such as the hybrid DFT-MD Car-Parrinello method [9], or the reactive MD force fields [10, 11].

The MD method has increasingly been incorporated in the Finite Element Method (FEM) framework [12–23] as the equilibrium equations of MD and FEM may be expressed in equivalent forms. The resulting Atomistic Finite Element Method (AFEM) [13], also referred to as Molecular Dynamic Finite Element Method (MDFEM) [24], is both computationally more favourable than MD [25], and offers a significant increase in compatibility and integrability with larger scale continuum FEM simulations. Structural mechanics elements (e.g. trusses, beams) have been used to analyse the overall mechanical behaviour of nano-scale entities, such as carbon nanotubes (CNT) [26–28], as well as the deformation of individual bonds [12, 14].

MDFEM is mostly applied to carbon nano-structures due to the maturity of carbon-specific force fields and the large interest in graphene, CNTs, and other fullerene derived compounds. However, non-carbon applications have been reported for other nano-structures, such as particulate metal matrix nano-composites [22] or boron-nitride nanotubes [23].

Several comprehensive presentations and reviews of AFEM/MDFEM and its implementations are available [24, 25, 29, 30]. Nonetheless, MDFEM remains a non-consolidated method because formal derivations are scarce, with significant differences arising on the topologies of the required MDEFM-specific elements. The available MDFEM element designs vary considerably in complexity and their implementation is often not straight-forward [16,21,25]. Additionally, only few proposed MDFEM element topologies are fully non-linear and non-local capable. This has lead to MDFEM often being implement using readily available, standard structural FEM elements such as beams, trusses and springs [12, 14, 20, 31, 32]. However, the use of structural elements results in the following detrimental restrictions of MDFEM's full non-linear capabilities:

1. *Inadequate Element Topologies with Limited Non-Local Capabilities*
   Severe inconsistencies arise where non-local force fields are approximated with structural elements which are topologically not adequate to represent multi-body potentials involving three or more atoms. Alternatively, structural FEM elements, often featuring rotational degrees of freedom (DoF), are used although the definition of point angles for atoms is highly ambiguous.

2. *Limited Large Deformation Analysis Capabilities*
   The mechanical behaviour of structural elements is inherently different from that of atomic bonds, especially for large-deformation analyses. An attractive alternative is the use of non-linear springs to represent the potentials accurately for large strains. However, torsional springs for instance, require rotational DoF to be included in the model upon which they can act and they are unable to represent, for example, cross-deformation sub-potentials such as stretch-bend interactions.

3. *Inability to Perform Conformational Analyses*
   Structural FEM elements typically prevent MDFEM from being able to perform the often required relaxation or conformational analysis step prior to the load application. This is due to the FEM elements' default inability to incorporate knowledge of the *natural* bond characteristics (e.g. bond length, angles), which are, in all but the simplest geometries (e.g. planar graphene), different from the overall structure's *equilibrium positions*.

This paper presents a fully non-linear MDFEM model, based on appropriate MDFEM-specific element topologies. A formal derivation of the MDFEM equilibrium equations, from first principles, is presented in section 2. The formulation can accommodate any type of MD force field, from classical, non-reactive many-body and pair-wise potentials, to advanced adaptive reactive bond order force fields (section 3). The presented derivation intrinsically considers all geometric non-linear effects and is explicitly independent of ambiguous rotational DoF.

The equilibrium equation for the smallest, fully non-linear MDFEM element topology, which can represent the molecular force field potential or each of its constituent sub-potentials, is derived exactly in section 4.2, together with exact expressions for the required corresponding Hessians (tangent stiffnesses). The element topology designs, presented in section 4.3, are intentionally kept as small and comprehensive as possible.

Analogously to the separation, in FEM, between the element topologies and the material properties, section 4.5 demonstrates how this MDFEM formulation uncouples the molecular force field from the element topologies. Significant advantages for the implementation and the stability analysis of the presented MDFEM arise from this uncoupling approach (4.6) — most notably, the ability to differentiate between instabilities in the system due to the force field or chemical bond failure (constitutive instability) and those due to the geometry of the structure (geometrical instability).

A method for the straight-forward implementation of the relevant equations (sections 2, 4.2 and 4.5) with the given element topologies is described in sections 5.1 and 5.2. A brief overview of optimization techniques for the equations' numerical implementation is given in section 5.3.

The model is shown to identically reproduce MD predictions [33] of brittle fracture in CNT with defects (section 6.1). Additionally, conformational analyses of complex three-dimensional Pillared Graphene Structures (PGS) are presented in section 6.2. Conclusions about this MDFEM implementation are given in section 7.

2. EQUATIONS OF EQUILIRBRIUM

2.1. Hamilton's Principle and Lagrange's Equation

A variational statement of equilibrium for a discrete domain can formally be derived from Hamilton's principle, which subjected to a Legendre transform, leads to Lagrange's equation. For a non-relativistic analysis, the domain's kinetic energy, T, equals its kinetic co-energy, T^*, so that the dynamic equilibrium within a conservative potential field, V, without damping effects, may hence be stated as:

$$\frac{\mathrm{d}}{\mathrm{d}t}\left(\frac{\partial\left(T\left(\dot{\mathbf{q}}\right)\right)}{\partial\dot{\mathbf{q}}}\right)^{\mathrm{T}}+\left(\frac{\partial\left(V\left(\mathbf{q}\right)\right)}{\partial\mathbf{q}}\right)^{\mathrm{T}}=\frac{\mathrm{d}}{\mathrm{d}t}\left(\nabla_{\dot{\mathbf{q}}}\left(T\left(\dot{\mathbf{q}}\right)\right)\right)+\nabla_{\mathbf{q}}\left(V\left(\mathbf{q}\right)\right)=\mathbf{g}, \tag{1}$$

where the vector derivatives adhere to the numerator layout convention. The domain's n displacements, given in generalized coordinates, are denoted by $\mathbf{q}\in\mathbb{R}^{n\times1}$ and are defined relative to an unloaded equilibrium position $\mathbf{q}_0=\mathbf{0}$, while $\mathbf{g}\in\mathbb{R}^{n\times1}$ represents the corresponding generalized forces. The operator $\nabla_{\mathbf{v}}$ represents the gradient of a scalar function with respect to the vector $\mathbf{v}$, in the same dimensions as $\mathbf{v}$, i.e. $\nabla_{\mathbf{v}}={}^{\partial}/_{\partial\mathbf{v}^{\mathrm{T}}}=\left({}^{\partial}/_{\partial\mathbf{v}}\right)^{\mathrm{T}}$. Moreover, $\mathbf{q}$ is chosen such that the kinetic energy, T, may be explicitly dependent only on the generalized velocities, $\dot{\mathbf{q}}\in\mathbb{R}^{n\times1}$, i.e. $T=T\left(\dot{\mathbf{q}}\right)$.

2.2. From Lagrange's Equation to a discrete Finite Element Method

The translational displacements of all atoms in a global Cartesian coordinate system, $\mathbf{u}\in\mathbb{R}^{n\times1}$, constitutes a natural choice of $\mathbf{q}$ for a discrete particle domain. Hence, the generalized corresponding forces, denoted $\mathbf{f}\in\mathbb{R}^{n\times1}$, are a set of linear forces only. Rotational DoF with corresponding moments are inappropriate quantities as atoms represent point particles. Using the choice $\mathbf{q}=\mathbf{u}$, equation (1) becomes:

$$\frac{\mathrm{d}}{\mathrm{d}t}\left(\nabla_{\dot{\mathbf{u}}}\left(T\left(\dot{\mathbf{u}}\right)\right)\right)+\nabla_{\mathbf{u}}\left(V\left(\mathbf{u}\right)\right)=\mathbf{f}. \tag{2}$$

The rest state of the atomic domain, when $\mathbf{u}=\mathbf{u}_0=\mathbf{0}$, is fully defined by the equilibrium positions of all ${}^{n}/_{3}$ atoms, denoted by $\mathbf{x}\in\mathbb{R}^{n\times1}$. Any deformed state of the domain may hence be described by $\mathbf{r}=\mathbf{x}+\mathbf{u}$, see figure 1.

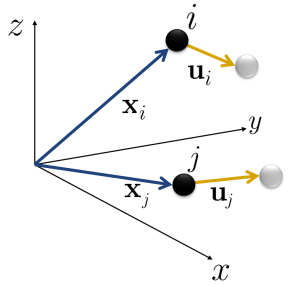

Figure 1. Coordinate System and Displacements Definitions for Atoms i and j

In the framework of Newtonian mechanics, the kinetic energy, T, for a domain constituted of point masses as defined in figure 1, can be expressed as:

$$T\left(\dot{\mathbf{u}}\right) = \frac{1}{2}\dot{\mathbf{u}}^{\mathrm{T}}\mathbf{M}\dot{\mathbf{u}}, \tag{3}$$

where the mass matrix, $\mathbf{M}$, is diagonal. Equation (2) may hence be expressed as:

$$\mathbf{M}\ddot{\mathbf{u}} + \nabla_{\mathbf{u}}\left(V\left(\mathbf{u}\right)\right) = \mathbf{f}, \tag{4}$$

where $\nabla_{\mathbf{u}}\left(V\left(\mathbf{u}\right)\right)$ is the transpose of the potential's Jacobian relative the the domain's displacements, i.e.$\nabla_{\mathbf{u}}\left(V\left(\mathbf{u}\right)\right) = \left(\mathbf{J}_{\mathbf{u}}^{V}\right)^{\mathrm{T}}$, such that global equilibrium, equation (4), may be equivalently expressed as:

$$\mathbf{M}\ddot{\mathbf{u}} + \left(\mathbf{J}_{\mathbf{u}}^{V}\right)^{\mathrm{T}} = \mathbf{f}. \tag{5}$$

Equation (5) is typical for a Finite Element Method framework and can be solved using a Newton-Raphson scheme provided the Hessian of the potential, expressed as:

$$\mathbf{H}_{\mathbf{u}}^{V} = \frac{\partial\left(\nabla_{\mathbf{u}}\left(V\left(\mathbf{x},\mathbf{u}\right)\right)\right)}{\partial\mathbf{u}}, \tag{6}$$

can be determined.

3. MOLECULAR FORCE FIELDS

3.1. Constituent Sub-Potentials

In general, a molecular force field, V, consists of the superposition of sub-potentials, V_S, as:

$$V\left(\mathbf{c}\right) = \sum_{\mathbb{S}} V_S\left(\mathbf{c}_S\right), \tag{7}$$

where $\mathbb{S}$ represents the set of included sub-potentials, $\mathbf{c} \in \mathbb{R}^{m\times 1}$ represents the m characteristic variables (e.g. bond lengths and angles) and $\mathbf{c}_S \in \mathbb{R}^{m_S\times 1}$ denotes the m_S specific characteristic variables required for evaluating the sub-potential V_S.

In general, classical force fields include sub-potentials for specific deformation modes such as bond stretching, bending and torsion, while more elaborate force fields may feature additional sub-potentials for mixed-mode deformations such as stretch-stretch, stretch-bend or bend-bend interactions [6]. Both non-reactive force fields and reactive bond-order force fields may be expressed in the form of equation (7). The many-body coupling bond-order variable, which is required in reactive fields (usually denoted b or B [10, 11]), may be also interpreted as a characteristic variable. Classical MD sub-potentials (e.g. stretch, bend, torsion) tend

to depend on a single characteristic variable only, $m_S = 1$, while cross-deformation sub-potentials (e.g. stretch-bend) may depend on two or more variables, $m_S > 1$. The non-reactive Lobo-Keating (fullerene-specific) force field for instance, may be stated as [34]:

$$\begin{aligned} V_{\text{Lobo-Keating}} &= V_{\text{S}} + V_{\text{B}} + V_{\text{I}} \\ &= \frac{1}{2}\sum_{i=1}^{n/3}\sum_{j=1}^{3}\frac{\alpha}{4r_0^2}\left(\mathbf{r}_{ij}\cdot\mathbf{r}_{ij} - r_0^2\right)^2 + \sum_{i=1}^{n/3}\sum_{j=1}^{2}\sum_{k=j+1}^{3}\frac{\beta}{r_0^2}\left(\mathbf{r}_{ij}\cdot\mathbf{r}_{ik} + \frac{1}{2}r_0^2\right)^2 + \quad (8) \\ &+ \sum_{i=1}^{n/3}\gamma\left(\mathbf{d}_i\cdot\mathbf{d}_i\right), \quad (9) \end{aligned}$$

where V_{S}, V_{B} and V_{I} refer to the stretch, bend and inversion sub-potentials respectively. The vector from atom i to atom j in the deformed state is denoted $\mathbf{r}_{ij} = \mathbf{r}_j - \mathbf{r}_i$. The natural bond length is given as r_0, and $\mathbf{d}_i$ represents the *dangling vector*, which is defined as $\mathbf{d}_i = \mathbf{r}_{i1} + \mathbf{r}_{i2} + \mathbf{r}_{i3}$. The force field's fitting parameters are α, β and γ. As another example, the MM3 (general-purpose) force field may be expressed as [6]:

$$V_{\text{MM3}} = V_{\text{S}} + V_{\text{B}} + V_{\text{T}} + V_{\text{SB}} + V_{\text{TS}} + V_{\text{TB}} + V_{\text{BB}} + V_{\text{VDW}}, \quad (10)$$

where V_{T}, V_{SB}, V_{TS}, V_{TB}, V_{BB} and V_{VDW} refer to the sub-potential energies of the torsion, stretch-bend, torsion-stretch, torsion-bend, bend-bend and Van der Waals interactions respectively. The reader is referred to [6] for the detailed sub-potential expressions.

A particularly interesting reactive force field is the Brenner potential [10, 11], which is of the form:

$$V = \sum_{i=1}^{n/3}\sum_{j>i}^{n/3}\left[V_{\text{R}}\left(r_{ij}\right) - \bar{B}_{ij}V_{\text{A}}\left(r_{ij}\right)\right], \quad (11)$$

where V_{R} and V_{A} represent the repulsive and attractive atomic interactions. The bond order, $\bar{B}_{ij}$, is a highly non-linear function of the bond angles centred at atoms i and j, the coordination number of atoms i and j as well as the coordination numbers of the first and second neighbour atoms to i and j.

3.2. Characteristic Variables

The force field's characteristic variables, $\mathbf{c}$, may always be expressed in the form $\mathbf{c} = \mathbf{c}\left(\mathbf{x}, \mathbf{u}\right)$, so that it is possible to reformulate the potential explicitly as:

$$V\left(\mathbf{c}\left(\mathbf{x}, \mathbf{u}\right)\right) = \sum_{\mathbb{S}} V_S\left(\mathbf{c}_S\left(\mathbf{x}, \mathbf{u}\right)\right) = \sum_{\mathbb{S}} V_S\left(\mathbf{x}, \mathbf{u}\right). \quad (12)$$

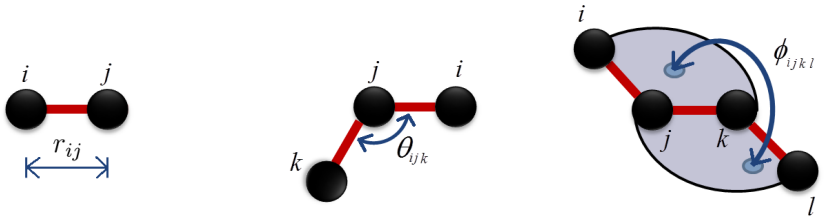

(a) Bond Stretching (b) Bond Bending (c) Bond Torsion

Figure 2. Characteristic Variables of Force Field Potentials

Figure 2 outlines a selection of common characteristic variables used by a variety of force fields. For instance, r_{ij} and θ_{ijk} in figure 2 are respectively given by:

$$r_{ij} = \|\mathbf{r}_j - \mathbf{r}_i\| = \|\mathbf{x}_j + \mathbf{u}_j - \mathbf{x}_i - \mathbf{u}_i\|, \tag{13}$$

$$\theta_{ijk} = \arccos\left(\frac{\mathbf{r}_{ji} \cdot \mathbf{r}_{jk}}{r_{ij} r_{jk}}\right) = \arccos\left(\frac{(\mathbf{x}_i + \mathbf{u}_i - \mathbf{x}_j - \mathbf{u}_j) \cdot (\mathbf{x}_k + \mathbf{u}_k - \mathbf{x}_j - \mathbf{u}_j)}{\|\mathbf{x}_i + \mathbf{u}_i - \mathbf{x}_j - \mathbf{u}_j\| \|\mathbf{x}_k + \mathbf{u}_k - \mathbf{x}_j - \mathbf{u}_j\|}\right). \tag{14}$$

A vast literature giving variable-defining sketches, such as in figure 2, is available and the reader is referred to [35] for a comprehensive collection.

4. MOLECULAR DYNAMIC FINITE ELEMENT METHOD

4.1. Introduction

In some cases, force field potentials may be represented exactly or approximately by FEM structural elements. However, the use of structural elements leads to significant restrictions, as outlined in section 1. In any case, it is possible to deduce a non-linear accurate representation of equation (5) within FEM through defining individual elements for each sub-potential as outlined in this section.

4.2. Constituent Sub-Hessian Matrices

Taking advantage of the sub-potential nature of force fields, equation (7), the total domain's Jacobian, $\mathbf{J}_{\mathbf{u}}^{V}$ in equation (5), and Hessian, $\mathbf{H}_{\mathbf{u}}^{V}$ in equation (6), can be obtained as:

$$\mathbf{J}_{\mathbf{u}}^{V}(\mathbf{x}, \mathbf{u}) = \frac{\partial V(\mathbf{x}, \mathbf{u})}{\partial \mathbf{u}} = \sum_{\mathbb{S}} \frac{\partial V_S(\mathbf{x}, \mathbf{u})}{\partial \mathbf{u}} = \sum_{\mathbb{S}} \mathbf{J}_{\mathbf{u}}^{V_S}(\mathbf{x}, \mathbf{u}). \tag{15}$$

$$\mathbf{H}_{\mathbf{u}}^{V}(\mathbf{x}, \mathbf{u}) = \frac{\partial (\nabla_{\mathbf{u}} (V(\mathbf{x}, \mathbf{u})))}{\partial \mathbf{u}} = \sum_{\mathbb{S}} \frac{\partial (\nabla_{\mathbf{u}} (V_S(\mathbf{x}, \mathbf{u})))}{\partial \mathbf{u}} = \sum_{\mathbb{S}} \mathbf{H}_{\mathbf{u}}^{V_S}(\mathbf{x}, \mathbf{u}). \tag{16}$$

Equations (15) and (16) show how the total potential, V, Jacobian, $\mathbf{J}_{\mathbf{u}}^{V}$, and Hessian, $\mathbf{H}_{\mathbf{u}}^{V}$, of the overall domain, Ω, may be divided into superimposed sub-domains, Ω_S, as shown in figure 3. It follows naturally that an element topology may be created for each individual

sub-potential, $V_S\left(\mathbf{c}_S\left(\mathbf{x},\mathbf{u}\right)\right)$, which is able to supply the necessary characteristic variables $\mathbf{c}_S\left(\mathbf{x},\mathbf{u}\right)$. These element types are then superposed when meshing the atomic domain. The spacial superposition of multiple element types outlines a first fundamental difference between the proposed MDFEM and the classical FEM, as in the latter, element superpositioning in the same location is atypical.

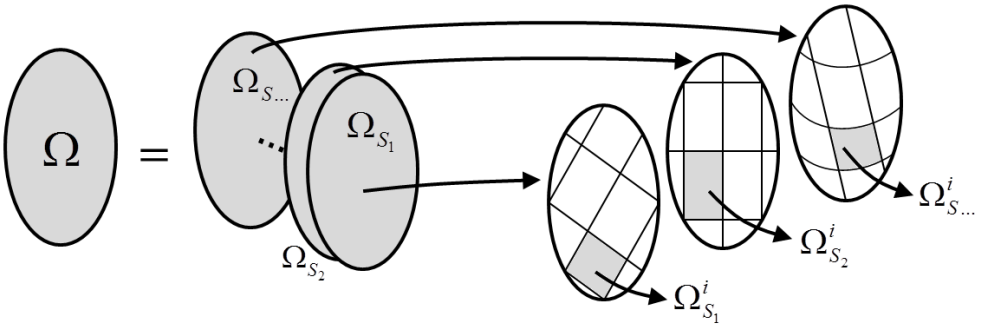

Figure 3. Illustration of Domain Decomposition and Sub-Domain Partitioning

For each sub-potential, V_S, the corresponding sub-domain, Ω_S, may in turn be divided into p_S partitions (figure 3), where $V_S^i \equiv V_S$ in partition i and is zero elsewhere. In general the partitioning pattern varies for different sub-potential domains, Ω_S (i.e. some sub-potentials require information from more atoms than others, see figure 4). It follows that the sub-potential may be then expressed as the summation over the partitions:

$$V_S\left(\mathbf{x},\mathbf{u}\right) = \sum_i^{p_S} V_S^i\left(\mathbf{x}_S^i,\mathbf{u}_S^i\right), \tag{17}$$

where $\mathbf{x}_S^i \in \mathbb{R}^{n_S\times 1}$ and $\mathbf{u}_S^i \in \mathbb{R}^{n_S\times 1}$ are the n_S components of $\mathbf{x}$ and $\mathbf{u}$ respectively which are necessary for evaluating V_S^i. Equation (17) indicates that p_S number of elements are needed for each sub-potential and that these elements must include the necessary atoms to supply $\mathbf{x}_S^i$ and $\mathbf{u}_S^i$. It follows that $\mathbf{H}_{\mathbf{u}}^{V_S}$ and $\mathbf{J}_{\mathbf{u}}^{V_S}$ may be obtained by first evaluating:

$$\mathbf{J}_{\mathbf{u}_S^i}^{V_S^i}\left(\mathbf{x}_S^i,\mathbf{u}_S^i\right) = \frac{\partial V\left(\mathbf{x}_S^i,\mathbf{u}_S^i\right)}{\partial \mathbf{u}_S^i} \quad \text{and} \quad \mathbf{H}_{\mathbf{u}_S^i}^{V_S^i}\left(\mathbf{x}_S^i,\mathbf{u}_S^i\right) = \frac{\partial\left(\nabla_{\mathbf{u}_S^i}\left(V_S^i\left(\mathbf{x}_S^i,\mathbf{u}_S^i\right)\right)\right)}{\partial \mathbf{u}_S^i}, \tag{18}$$

followed by an assembling of equations (18) of the type:

$$\mathbf{J}_{\mathbf{u}}^{V_S}\left(\mathbf{x},\mathbf{u}\right) = \sqcup_{p_S}^{V_S}\left(\mathbf{J}_{\mathbf{u}_S^i}^{V_S^i}\left(\mathbf{x}_S^i,\mathbf{u}_S^i\right)\right) \quad \text{and} \quad \mathbf{H}_{\mathbf{u}}^{V_S}\left(\mathbf{x},\mathbf{u}\right) = \sqcup_{p_S}^{V_S}\left(\mathbf{H}_{\mathbf{u}_S^i}^{V_S^i}\left(\mathbf{x}_S^i,\mathbf{u}_S^i\right)\right), \tag{19}$$

where $\sqcup_{p_S}^{V_S}$ denotes the assembly operator which assembles the contributions of all p_S Jacobians, $\mathbf{J}_{\mathbf{u}_S^i}^{V_S^i}\left(\mathbf{x}_S^i,\mathbf{u}_S^i\right) \in \mathbb{R}^{1\times n_S}$, into the corresponding positions within $\mathbf{J}_{\mathbf{u}}^{V_S}\left(\mathbf{x},\mathbf{u}\right) \in \mathbb{R}^{1\times n}$ and similarly the contributions of of all p_S Hessians, $\mathbf{H}_{\mathbf{u}_S^i}^{V_S^i}\left(\mathbf{x}_S^i,\mathbf{u}_S^i\right) \in \mathbb{R}^{n_S\times n_S}$, into $\mathbf{H}_{\mathbf{u}}^{V_S}\left(\mathbf{x},\mathbf{u}\right) \in \mathbb{R}^{n\times n}$.

The numerical solution to the global equilibrium problem, equation (5), using an iterative solution scheme requiring the Hessian (equation (6)), can therefore be obtained trivially using equations (18) and (19) together with suitable element topologies.

4.3. Element Topologies

The topology of the elements required for each sub-potential is determined by the respective components of $\mathbf{c}_S$. The most compact and comprehensive element designs are hence identical to the characteristic variable-defining sketches for each force field (fig. 2). Figure 4 features a set of basic element shapes used for non-reactive and reactive force fields. Elements for reactive force fields include more atoms as the bond-order characteristic has a higher non-locality.

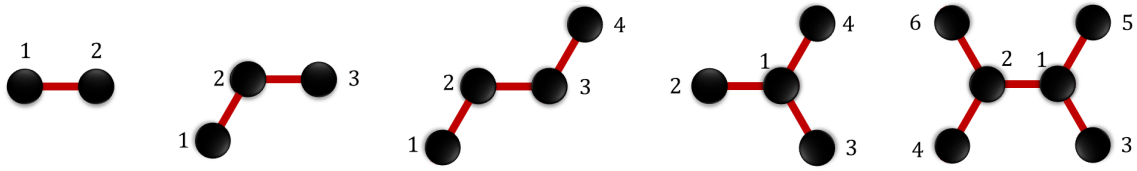

(a) NR-2 (b) NR-3 (c) NR-4-C (d) NR-4-S (e) R-6

Figure 4. Selection of Non-Reactive (NR) and Reactive (R) Element Topologies

Table 1 outlines a small selection of characteristic variables which the elements in figure 4 can supply and which sub-potentials they may be required for.

Table 1. Element Topologies, Characteristic Variables, $\mathbf{c}_S$, and Applicable Sub-Potentials, V_S.

NR-2	NR-3	NR-4-C	NR-4-S
$r_{12} = \sqrt{\mathbf{r}_{12} \cdot \mathbf{r}_{12}}$	$r_{21} = \sqrt{\mathbf{r}_{21} \cdot \mathbf{r}_{21}}$	$\cos(\phi_{1234}) = -\hat{\mathbf{r}}_{123} \cdot \hat{\mathbf{r}}_{234}$	$d_1^2 = \mathbf{d}_1 \cdot \mathbf{d}_1$
$r_{12}^2 = \mathbf{r}_{12} \cdot \mathbf{r}_{12}$	$(r_{21} r_{23} \cos(\theta_{123})) = \mathbf{r}_{21} \cdot \mathbf{r}_{23}$	$\hat{\mathbf{r}}_{123} = \left(\frac{\mathbf{r}_{12} \times \mathbf{r}_{23}}{r_{12} r_{23}} \right)$	$d_1 = \sqrt{\mathbf{d}_1 \cdot \mathbf{d}_1}$
V_S, V_{VDW}	V_B, V_{SB}, V_{SS}	V_T, V_{TS}, V_{TB}	V_I, V_{IT}, V_{BB}

S = Stretch, B = Bend, T = Torsion, I = Inflexion, IT = Improper Torsion, SS = Stretch-Stretch
SB = Stretch-Bend, BB = Bend-Bend, TS = Torsion-Stretch, TB = Torsion-Bend, VDW = Van der Waals

Reactive element topologies require at least six atoms (e.g. R-6), three on each side of the bond [10, 11], while as many as fourteen may be required in case that coordination numbers above three are considered. In general, larger elements share characteristic variables with smaller element, so that they could represent the smaller element's sub-potential as well. However, this approach is to be discouraged because larger element topologies cannot be meshed as close to the domain boundary as smaller topologies, leading to increased edge effects. Finally, it can be noted that since the characteristic variables are defined in a global frame of reference (FoR), these elements do not require a local to global reference frame transformation prior to assembly.

4.4. Derivation of the Element Jacobian and Hessian

Implementing the elements of section 4.3 within the Finite Element Method requires deriving each element's contribution to the global equilibrium equations, equation (5), i.e $\mathbf{J}_{\mathbf{u}_S^i}^{V_S^i}$, as well as deriving $\mathbf{H}_{\mathbf{u}_S^i}^{V_S^i}$, which is required for the iterative solution scheme. Modern interpreted processing languages are increasingly capable of rapid symbolic derivation of analytical expressions so that the Jacobian and Hessian may be generated symbolically. This process for an element type, omitting the i and S indices for clarity of notation, may be represented by:

$$\left\{V_S\left(\mathbf{c}\right), \mathbf{x}, \mathbf{u}, \mathbf{c}\left(\mathbf{x}, \mathbf{u}\right)\right\} \rightarrow \text{Symbolic Processor} \rightarrow \left\{\mathbf{H}_{\mathbf{u}}^{V_S}, \mathbf{J}_{\mathbf{u}}^{V_S}\right\}. \tag{20}$$

The computational effort for this process is small; however, the resulting expression for a single entry of the Hessian, $\left(H_{\mathbf{u}_S}^{V_S}\right)_{i,j}$, can become prohibitively long for the implementation in a compilable language (e.g. the FORTRAN 90/95 standard has a maximum of 5148 characters per statement, although specific compilers may offer higher limits). These excessively long derivatives easily occur for higher-order sub-potentials requiring elements with $n_S > 6$, or where $\mathbf{c}_S$ requires more complex functions such as inverse trigonometric relations.

More aggravatingly, the direct evaluation of $\mathbf{J}_{\mathbf{u}_S^i}^{V_S^i}$ and $\mathbf{H}_{\mathbf{u}_S^i}^{V_S^i}$ compounds the element topology information with that of the implemented force field. Force field characteristics and element topology properties may be kept uncoupled, section 4.5, resulting in a significantly increased flexibility of this MDFEM formulation in combining different element types for different potentials.

4.5. Decoupling Element Topology and Force Field

Noting equation (12), each entry in the sub-potential's Jacobian and Hessian tensors, $\left(J_{\mathbf{u}}^{V_S}\right)_{i,j}$ and $\left(H_{\mathbf{u}}^{V_S}\right)_{i,j}$ in equation (18), may equivalently be expressed as:

$$\begin{aligned}\left(J_{\mathbf{u}}^{V_S}\right)_{1,i} = \frac{\partial V_S}{\partial u_i} &= \sum_{k=1}^{m_S} \frac{\partial V_S}{\partial c_k}\frac{\partial c_k}{\partial u_i} \\ &= \sum_{k=1}^{m_S} \left(J_{\mathbf{c}}^{V_S}\right)_{1,k} \left(J_{\mathbf{u}}^{\mathbf{c}}\right)_{k,i},\end{aligned} \tag{21}$$

$$\begin{aligned}\left(H_{\mathbf{u}}^{V_S}\right)_{i,j} = \frac{\partial^2 V_S}{\partial u_i \partial u_j} &= \sum_{k=1}^{m_S} \frac{\partial c_k}{\partial u_i}\left(\sum_{l=1}^{m_S} \frac{\partial^2 V_S}{\partial c_k \partial c_l}\frac{\partial c_l}{\partial u_j}\right) + \sum_{k=1}^{m_S} \frac{\partial V_S}{\partial c_k}\frac{\partial^2 c_k}{\partial u_i \partial u_j} \\ &= \sum_{k=1}^{m_S} \left(J_{\mathbf{u}}^{\mathbf{c}}\right)_{k,i}\left(\sum_{l=1}^{m_S} \left(H_{\mathbf{c}}^{V_S}\right)_{k,l}\left(J_{\mathbf{u}}^{\mathbf{c}}\right)_{l,j}\right) + \sum_{k=1}^{m_S} \left(J_{\mathbf{c}}^{V_S}\right)_{1,k}\left(H_{\mathbf{u}}^{\mathbf{c}}\right)_{k,i,j},\end{aligned} \tag{22}$$

where $\mathbf{J}_{\mathbf{c}}^{V_S} \in \mathbb{R}^{1\times m_S}$ and $\mathbf{H}_{\mathbf{c}}^{V_S} \in \mathbb{R}^{m_S\times m_S}$ are the sub-potential's respective Jacobian and Hessian tensors relative to the characteristic variables. Similarly, $\mathbf{J}_{\mathbf{u}}^{\mathbf{c}} \in \mathbb{R}^{m_S\times n_S}$ and $\mathbf{H}_{\mathbf{u}}^{\mathbf{c}} \in$

$\mathbb{R}^{m_S \times n_S \times n_S}$ are the Jacobian and Hessian tensors of the characteristic variables relative to the element nodal DoF. The process in equation (20) may thus be restated as:

$$\left\{V_S\left(\mathbf{c}\right), \mathbf{x}, \mathbf{u}, \mathbf{c}\left(\mathbf{x}, \mathbf{u}\right)\right\} \rightarrow \text{Symbolic Processor} \rightarrow \left\{\mathbf{J}_{\mathbf{c}}^{V_S}, \mathbf{H}_{\mathbf{c}}^{V_S}, \mathbf{J}_{\mathbf{u}}^{\mathbf{c}}, \mathbf{H}_{\mathbf{u}}^{\mathbf{c}}\right\}, \tag{23}$$

which may then be used to directly generate the compilable language script as:

$$\begin{aligned}\left\{\mathbf{J}_{\mathbf{c}}^{V_S}, \mathbf{H}_{\mathbf{c}}^{V_S}, \mathbf{J}_{\mathbf{u}}^{\mathbf{c}}, \mathbf{H}_{\mathbf{u}}^{\mathbf{c}}, \text{Eq. (21)-(22)}\right\} &\rightarrow \text{Interpreted Language} \rightarrow \\ &\rightarrow \left\{\mathbf{H}_{\mathbf{u}}^{V_S},\ \mathbf{J}_{\mathbf{u}}^{V_S}, \text{in a compilable language}\right\}.\end{aligned} \tag{24}$$

4.6. Stability and Implementation Advantages of Uncoupling Force Fields and Element Topologies

Equations (21) and (22), hereafter termed *reconstruction equations*, result in the following advantages:

1. *Reduced Complexity of Derivatives*
   The *reconstruction equations* require the symbolic evaluation of more, yet shorter derivatives so that the latter may be more comfortably implemented in a compilable language script. Additionally, the computational effort for the iterative solver reduces because less operations are required to evaluate $\mathbf{H}_{\mathbf{u}}^{V_S}$ and $\mathbf{J}_{\mathbf{u}}^{V_S}$ by using the *reconstruction equations* than by a direct approach.

2. *Separation of Force Field Potentials from Element Topologies*
   The force field sub-potentials become completely uncoupled from the element types so that a library of pre-compiled derivatives for both the force fields on one hand, and the elements on the other hand, can be developed and stored separately.

3. *Independent Scaling of Derivatives' Length*
   The above uncoupling also results in entries of $\mathbf{J}_{\mathbf{c}}^{V_S}, \mathbf{H}_{\mathbf{c}}^{V_S}$, $\mathbf{J}_{\mathbf{u}}^{\mathbf{c}}$ and $\mathbf{H}_{\mathbf{u}}^{\mathbf{c}}$ to scale in length only with either the complexity of $V_S\left(\mathbf{c}\right)$ or $\mathbf{c}\left(\mathbf{x}, \mathbf{u}\right)$ respectively, but any compound effect is avoided. The only condition for selecting an element type for a sub-potential is that the element must be able to supply all characteristic variables required by V_S.

4. *Independent Analysis of Constitutive and Geometrical Instabilities*
   Finally, and perhaps most importantly, the *reconstruction equations* allow for an analysis of the two structural instabilities which may occur during MDFEM simulations. The first is a *geometrical instability*, which occurs for instance during buckling. The second is a *chemical-constitutive instability*, which can arise if the force field's potential features an inflexion point. In this case, the Hessian tensor (tangent stiffness) will cease to be positive-definite and negative eigenvalues may appear in the solution procedure.

   A guaranteed identification of a *constitutive instability* cannot be achieved by considering $\mathbf{H}_{\mathbf{u}}^{V_S}$ directly. In general, an MDFEM element is geometrically under-determined

in some directions of global space, so that the latter's geometrical under-determination masks the chemical bond yielding in the overall Hessian, $\mathbf{H}_{\mathbf{u}}^{V_S}$.

However, *constitutive instabilities* can readily be detected by testing for positive-definiteness of $\mathbf{H}_{\mathbf{c}}^{V_S}$. An expensive eigenvalue analysis to test for the positive-definite nature of $\mathbf{H}_{\mathbf{c}}^{V_S}$ can be avoided by recognizing that it is a Hermitian matrix and thus Sylvester's criterion may be applied.

5. IMPLEMENTATION

5.1. Numerical Implementation of Global Equilibrium

The presented formulation was implemented symbolically in MATLAB [36], and the resultant formulations were exported in a FORTRAN format, which is suitable for the FE package ABAQUS [37]. The latter allows for the definition of customized element types, termed *User Elements*, with freely definable element topologies and constitutive properties. A FORTRAN subroutine (UEL), which takes the nodal variables $(\mathbf{x}, \mathbf{u})$ as input, must supply the elements' Jacobian, $\mathbf{J}_{\mathbf{u}}^{V_S}$, and Hessian, $\mathbf{H}_{\mathbf{u}}^{V_S}$, to the FEM solver. A flowchart of the overall implementation including pre-processing (e.g. symbolic derivations, atom seeding, element meshing) is presented in section 5.2, while section 5.3 covers additional optimization performed on the generated subroutine using Common Subexpression Elimination (CSE).

5.2. Preprocessing

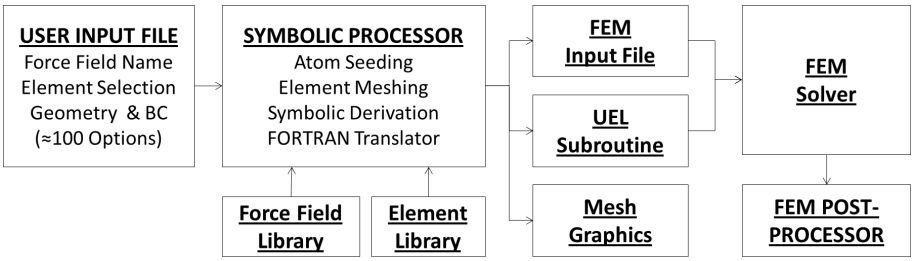

Figure 5. Implementation Pre-Processor and Solver

A symbolic pre-processor (fig. 5) generates all required files for implementing the current MDFEM within the FEM. The user input file must define the choice of force field and element topologies, the atomic geometry and the boundary conditions (BC); additional advanced options, such as periodic boundary conditions or optimization techniques are available.

The requested geometry is seeded and meshed with all required element types before the element types' Jacobians, $\mathbf{J}_{\mathbf{c}}^{V_S}(\mathbf{x}, \mathbf{u})$, $\mathbf{J}_{\mathbf{u}}^{\mathbf{c}}(\mathbf{x}, \mathbf{u})$, and Hessians, $\mathbf{H}_{\mathbf{c}}^{V_S}(\mathbf{x}, \mathbf{u})$, $\mathbf{H}_{\mathbf{u}}^{\mathbf{c}}(\mathbf{x}, \mathbf{u})$, are derived symbolically. The latter are translated into FORTRAN language, CSE optimized and then combined with the *reconstruction equations* (21) and (22) in the UEL subroutine script.

The Element Library contains the characteristic variable definitions, $\mathbf{c} = \mathbf{c}(\mathbf{x}, \mathbf{u})$, and node connectivities of each element type. The force field library contains the force field definitions in the form $V(\mathbf{c}) = \sum_{\mathbb{S}} V_S(\mathbf{c})$. Hence, the implementation of a new force field constitutes no additional time cost once an Element Library has been established.

5.3. Script-Level Local, Common Subexpression Elimination (CSE)

The characteristic variables' vectorized definitions, equations (13) and (14), result in expressions for the entries of the characteristic variables' Jacobian, $\mathbf{J}^{\mathbf{c}}_{\mathbf{u}}$, and Hessian, $\mathbf{H}^{\mathbf{c}}_{\mathbf{u}}$, which are ideally suited for local CSE optimization. While many compilers include CSE capability, it was chosen to implement CSE at the FORTRAN script level, especially because elaborate characteristic variables may still cause prohibitively long statement expressions (e.g. NR-4's $\cos(\phi_{ijkl}) = -\hat{\mathbf{r}}_{ijk} \cdot \hat{\mathbf{r}}_{jkl}$). In general, using a pre-computed temporary variable $t_0 = t_0(\mathbf{x}, \mathbf{u})$, an entry of the Hessian, $\mathbf{H}^{\mathbf{c}}_{\mathbf{u}}$, may be reformulated as:

$$\left(H^{\mathbf{c}}_{\mathbf{u}}\right)_{i,j,k} = h(\mathbf{x}, \mathbf{u}) = h_0(\mathbf{x}, \mathbf{u}, t_0), \tag{25}$$

where t_0 is chosen so as to maximize the length reduction of $h(\mathbf{x}, \mathbf{u})$. Subsequent temporary variables may use preceding temporary variables: $t_l = t_l(\mathbf{x}, \mathbf{u}, t_1, \ldots, t_{l-1})$ for $l > 1$, such that after l substitutions, the Hessian is evaluated as $\left(H^{\mathbf{c}}_{\mathbf{u}}\right)_{i,j,k} = h_l(\mathbf{x}, \mathbf{u}, t_0, \ldots, t_l)$. The temporary variables may be reused immediately after this evaluation, in order to keep the register allocation low. For the MM3 force field, this CSE results in an overall 80% reduction of mathematical operations, while the overall script length generally reduces by 73%.

6. APPLICATIONS

Two applications of the implemented MDFEM are presented. Firstly, the equivalence of MDFEM and MD is demonstrated using a static, non-linear fracture simulation of CNT. Secondly, non-equilibrium meshes of complex three-dimensional Pillared Graphene Structures (PGS) are allowed to relax, hence demonstrating the current implementation's capability to perform conformational analyses.

6.1. Brittle Failure of Carbon Nanotubes (CNT) with Defects

The MD study by Belytschko et al. [33], investigating the effects of defects on the fracture behaviour of CNT, was chosen as a reference to demonstrate the equivalence of MDFEM and MD in a highly non-linear environment up to, and including bond failure. Three CNT configurations [33] (table 2) were tested in a static analysis, $\ddot{\mathbf{u}} = \mathbf{0}$, and were strained axially to fracture. The effect of defects was included by softening a bond in the middle of the CNT by 10% (i.e. effectively a 0.9 multiplication factor was applied to both $\mathbf{J}^{V_S}_{\mathbf{u}}$ and $\mathbf{H}^{V_S}_{\mathbf{u}}$ of the affected elements). Failure of a bond is detected in the current MDFEM implementation by testing each bond's $\mathbf{H}^{V_S}_{\mathbf{c}}$ for positive-definiteness, as discussed in section 4.6. Following Belytschko et al. [33], the Brenner potential [10], equation (11), is approximated in this example by a Morse type potential of the form:

$$V = V_{\mathrm{S}} + V_{\mathrm{B}} = \alpha \left\{ \left[1 - e^{-\beta(r_{ij} - r_0)}\right]^2 - 1 \right\} + \frac{1}{2}\gamma \left(\theta_{ijk} - \theta_0\right)^2 \left[1 + \lambda \left(\theta_{ijk} - \theta_0\right)^4\right]. \tag{26}$$

The above potential was developed to be equivalent to the Brenner force field for strains up

to 10% [33], but without suffering from the subsequent *camel-back* problem in the force-displacement relation. The fitting constants for equation (26) are: $r_0 = 1.39$ Å, $\theta_0 = 2.094$ rad, $\alpha = 6.03105$ nN Å, $\beta = 2.625$ Å^{-1}, $\gamma = 9.0$ nN Å/rad^2 and $\lambda = 0.754$ rad^{-4} [33]. The present formulation identifies CNT uniquely by a triplet of integers, such as $(20, 0, 10)$. The first two indices, $(20, 0)$, refers to the commonly-used integer notations for the chiral vector, $\mathbf{C}_\text{h} = 20 \cdot \mathbf{a}_1 + 0 \cdot \mathbf{a}_2$, where $\mathbf{a}_1$ and $\mathbf{a}_1$ denote the graphene lattice vectors. The third index, 10, identifies the CNT height as $10 \cdot \|\mathbf{T}\|$, where $\mathbf{T}$ is the orthogonal translational vector [17, 38].

Table 2. Model Specifications - Brittle CNT Failure Simulations

CNT Configuration	Atoms	V_S Element	p_S	V_B Element	p_B	Equilibrium Length l_0 (Å)
(12,12,20)	984	NR-2	1452	NR-3	2855	48.151
(16,8,10)	1128	NR-2	1664	NR-3	3279	53.588
(20,0,10)	820	NR-2	1200	NR-3	2359	41.700

The geometries were constrained and displaced using two single rows of atoms, one at each end of the CNT, Ω_1 and Ω_2. Figure 6 highlights these edge atoms, the fixed ones on the left, $\mathbf{u}(\Omega_1) = \mathbf{0}$, and the displaced ones, Ω_2, on the right. The MDFEM used a direct sparse matrix solver. For comparison with literature, the stress-strain results are reported in conventional pressure units. The two-dimensional stress is normalized by assuming a CNT wall thickness, $t_\text{wall} = 3.4$ Å, as: $\sigma_\text{3D} = \dfrac{\sum_{\Omega_2} f_i}{A}$, where $A = t_\text{wall}\|\mathbf{C}_\text{h}\|$ and the strain is evaluated as $\epsilon = \dfrac{l - l_0}{l_0}$.

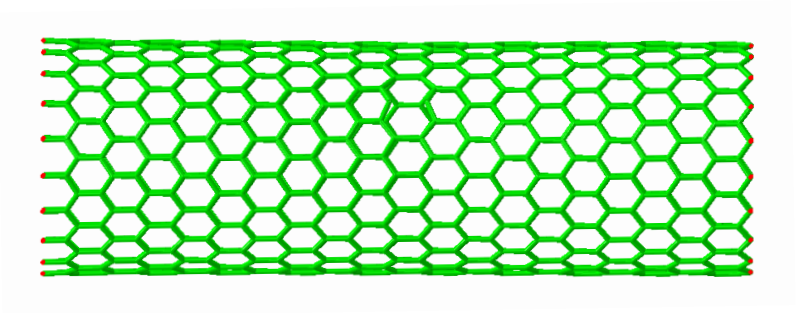

Figure 6. Displacement Boundary Domains of CNT (20,0,10)

Figure 7 demonstrates an excellent agreement between the current MDFEM implementation and the MD results reported in [33]. The predictions for failure strain and failure stress show no identifiable differences for the Zig-Zag CNTs, while for the Chiral and Armchair CNTs these are minor and negligible. Additionally, the brittle nature of the fracture can be deduced from MDFEM because no bonds had fully failed prior to global divergence. Figure 8 highlights the domain of the CNT which contains the softened bond at a global axial strain of 15.8%. All simulations took $\mathcal{O}(10^1 - 10^2)$ seconds to complete using a standard workstation running a 3.3 GHz Intel i5-2500 CPU.

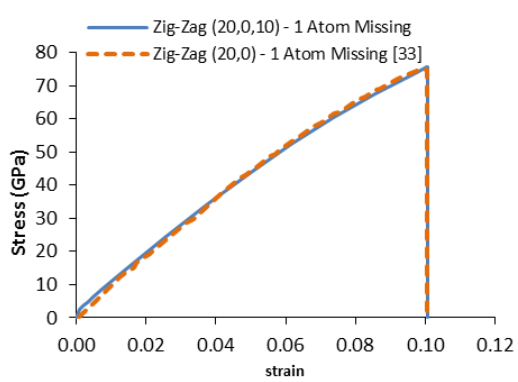

(a) CNT (20,0,10) With a Severe Vacancy Defect

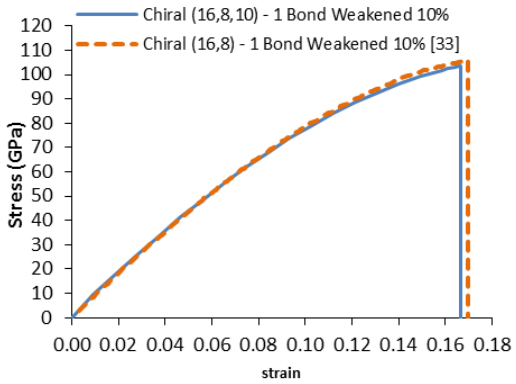

(b) CNT (16,8,4) With a Soft Bond Defect

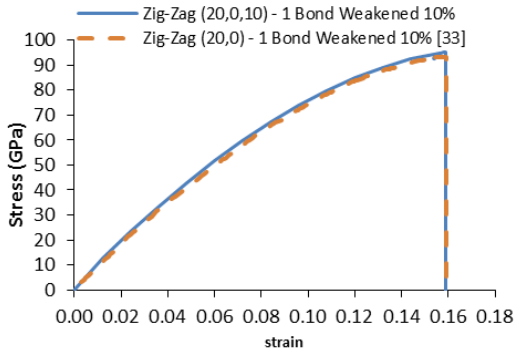

(c) CNT (20,0,10) With a Soft Bond Defect

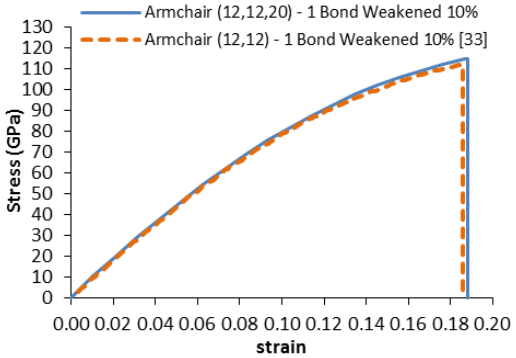

(d) CNT (12,12,20) With a Soft Bond Defect

Figure 7. Stress-Strain Behaviours of CNT of Varying Chirality with Defects

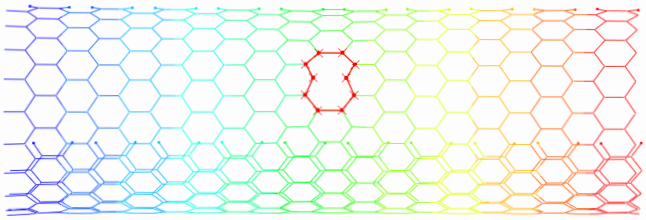

Figure 8. Cut-View of CNT (20,0,10) with Highlighted Softened Bond Region in an Axial Deformation Field at 15.8% Strain

6.2. Conformational Analysis: 3D Pillared Graphene Structure

The seeding of 3D Pillared Graphene Structure (PGS) meshes, such as the those in figures 9(a) and 9(c), is considerably more complex and computationally intensive than seeding SLGS or CNT [39–45]. A conformational analysis is typically required before any loading may be applied. Two examples are presented, the first being PGS-1, figure 9(a). This PGS is constituted of a single CNT of configuration (8,0,4), which is perpendicularly joined to SLGS at both its ends. The second example, PGS-2 in figure 9(c), is a more complex sample structure due to the close proximity of its two CNT which are of configurations (8,0,4) and (6,0,4).

Both the PGS-1 and PGS-2 configurations are potentially representative Unit Cell (UC) domains. These structures were equilibrated using the Lobo-Keating potential, equation (9), with the following fitting parameters [34]: $r_0 = 1.421$ Å, $\alpha = 15.59$ nN/Å , $\beta = 2.55$ nN/Å and $\gamma = 0.74$ nN/Å.

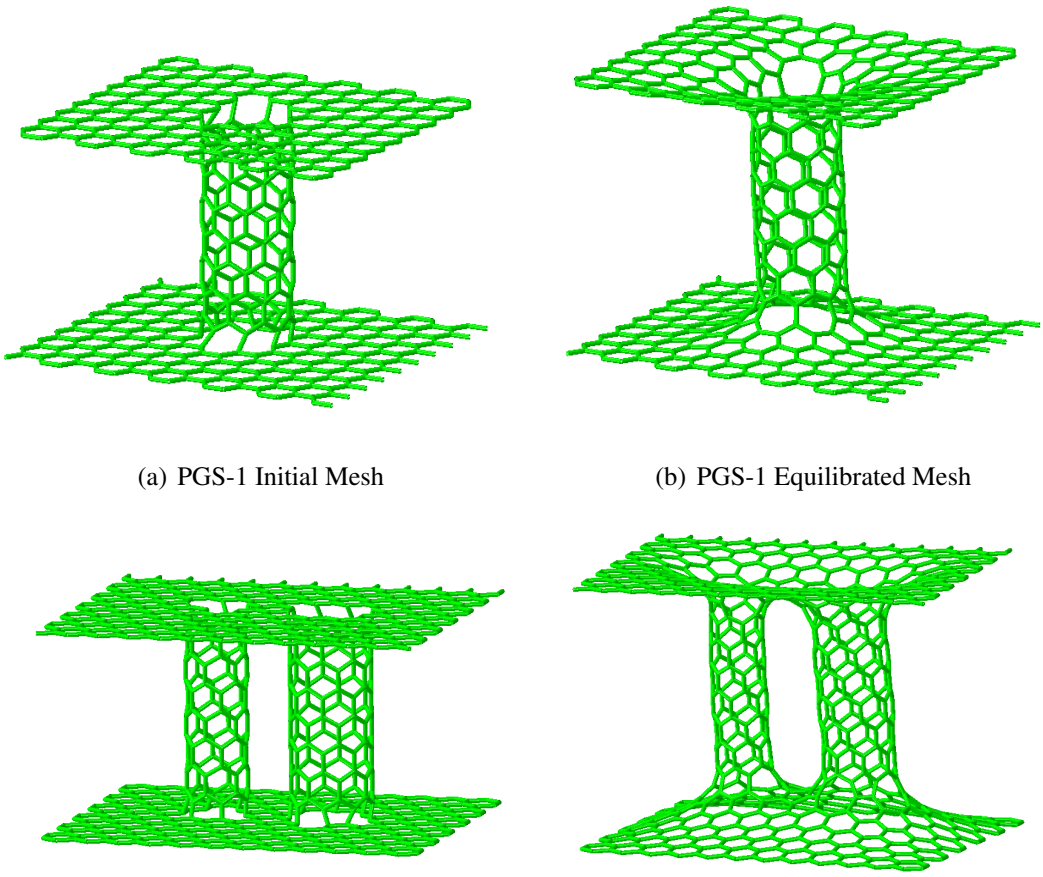

(a) PGS-1 Initial Mesh

(b) PGS-1 Equilibrated Mesh

(c) PGS-2 Initial Mesh

(d) PGS-2 Equilibrated Mesh

Figure 9. Conformational Analyses of Non-Equilibrium PGS Meshes

The equilibrated state of the PGS-1 in figure 9(b) and that of PGS-2 in figure 9(d), are easily obtained by prescribing $\mathbf{f} = \mathbf{0}$ and appropriate basic boundary conditions on the structures. The geometries relax to their energy minimizing configuration, as shown in figures 9(b) and 9(d).

Homogenized mechanical properties of PGS, obtained through an approximated MDFEM, are available [32], but the latter study required a full MD pre-processing step to obtain the conformational analysis prior to loading. Only force fields with strictly monotonic force-displacement relations (i.e. inflexion-free potentials) should be used in conformational analyses. This criterion almost always guarantees fast, problem-free convergence to an approximate energy minimum, which may be refined with a more precise force field around that energy minimum. Figure 9(d) demonstrates that the current MDFEM is able to perform conformational analyses on quite challenging geometries.

7. CONCLUSION

A mathematically rigorous, fully non-linear derivation and a comprehensive implementation of the Molecular Dynamic Finite Element Method (MDFEM) has been presented. The model has shown to yield numerical predictions identical to MD fracture simulations and has produced, to the best of the authors' knowledge, novel results by achieving the first fully MD-equivalent conformational analyses performed within MDFEM.

The formulation bases itself on the simplest possible MDFEM element topologies which are available throughout literature, and hence the force field characteristic variables are defined unambiguously. This intuitive and clear approach significantly facilitates the numerical implementation of MDFEM and should spark an increased use of the latter.

Moreover, the present MDFEM derivation uncouples the force field potentials from the element topologies in a way which is analogous to the separation of constitutive relations and element topologies in classical FEM. This approach further enhances the flexibility, clarity and accessibility of the present formulation. Solely the force field in its basic form, $V = V(\mathbf{c})$, and the definitions of the characteristic variables, $\mathbf{c} = \mathbf{c}(\mathbf{r}, \mathbf{u})$, are required as inputs to model the chosen MD force field exactly within MDFEM. Additionally, the *force field vs. element topology* uncoupling results in the current model's ability to differentiate explicitly between geometrical instabilities (e.g. buckling) and constitutive instabilities (e.g. bond failures) during the simulations.

Finally, the current model is ideally suited for multi-scale integration (hierarchical and concurrent) with larger-scale FEM simulations. The given derivation of MDFEM may equally well accommodate multi-physics effects if the element topologies are enriched with appropriate degrees of freedom beyond the current displacement DoF.

Acknowledgements

The present project is supported by the National Research Fund, Luxembourg (1360982)

Roshan Bhalla is acknowledged for generating the PGS meshes.

8. REFERENCES

[1] K. S. Novoselov, A. K. Geim, S. V. Morozov, D. Jiang, Y. Zhang, S. V. Dubonos, I. V. Grigorieva, and A. A. Firsov, "Electric field effect in atomically thin carbon films," *Science*, 306, 666–669, 2004.

[2] C. Chen, S. Rosenblatt, K. Bolotin, P. Kim, I. Kymissis, H. Stormer, T. Heinz, and J. Hone, "Nems applications of graphene," in *Electron Devices Meeting (IEDM), 2009 IEEE International*, 1 –4, dec. 2009.

[3] R. A. Barton, J. Parpia, and H. G. Craighead, "Fabrication and performance of graphene nanoelectromechanical systems," *Journal of Vacuum Science & Technology B: Microelectronics and Nanometer Structures*, 29, 050801, 2011.

[4] I. Pettersson and T. Liljefors, "Molecular mechanics calculated conformational energies of organic molecules: A comparison of force fields," 167–189, 2007.

[5] N. L. Allinger, "Conformational analysis. 130. mm2. a hydrocarbon force field utilizing v1 and v2 torsional terms," *Journal of the American Chemical Society*, 99, 8127–8134, 1977.

[6] N. L. Allinger, Y. H. Yuh, and J. H. Lii, "Molecular mechanics. the mm3 force field for hydrocarbons. 1," *Journal of the American Chemical Society*, 111, 8551–8566, 1989.

[7] D. Srivastava and et al., "Computational nanotechnology: A current perspective," *CMES*, 3, 531–538, 2002.

[8] S. Swaminarayan, K. Kadau, T. C. Germann, and G. C. Fossum, "369 tflop/s molecular dynamics simulations on the roadrunner general-purpose heterogeneous supercomputer," *SC Conference*, 0, 1–10, 2008.

[9] R. Car and M. Parrinello, "Unified approach for molecular dynamics and density-functional theory," *Phys. Rev. Lett.*, 55, 2471–2474, Nov 1985.

[10] D. W. Brenner, "Empirical potential for hydrocarbons for use in simulating the chemical vapor deposition of diamond films," *Phys. Rev. B*, 42, 9458–9471, Nov 1990.

[11] D. W. Brenner, O. A. Shenderova, J. A. Harrison, S. J. Stuart, B. Ni, and S. B. Sinnott, "A second-generation reactive empirical bond order (rebo) potential energy expression for hydrocarbons," *Journal of Physics: Condensed Matter*, 14, 783, 2002.

[12] G. M. Odegard, T. S. Gates, L. M. Nicholson, and K. E. Wise, "Equivalent-continuum modeling of nano-structured materials," tech. rep., NASA Technical Report, NASA/TM-2001-210863, May 2001.

[13] Y. Wang, C. Sun, X. Sun, J. Hinkley, G. M. Odegard, and T. S. Gates, "2-d nano-scale finite element analysis of a polymer field," *Composites Science and Technology*, 63, 1581 – 1590, 2003.

[14] C. Li and T.-W. Chou, "A structural mechanics approach for the analysis of carbon nanotubes," *International Journal of Solids and Structures*, 40, 2487 – 2499, 2003.

[15] X. Sun and W. Zhao, "Prediction of stiffness and strength of single-walled carbon nanotubes by molecular-mechanics based finite element approach," *Materials Science and Engineering: A*, 390, 366 – 371, 2005.

[16] L. Nasdala and G. Ernst, "Development of a 4-node finite element for the computation of nano-structured materials," *Computational Materials Science*, 33, 443 – 458, 2005.

[17] M. Meo and M. Rossi, "Prediction of young's modulus of single wall carbon nanotubes by molecular-mechanics based finite element modelling," *Composites Science and Technology*, 66, 1597 – 1605, 2006.

[18] K. Tserpes, P. Papanikos, and S. Tsirkas, "A progressive fracture model for carbon nanotubes," *Composites Part B: Engineering*, 37, 662 – 669, 2006.

[19] J. Xiao, J. Staniszewski, and J. G. Jr., "Fracture and progressive failure of defective graphene sheets and carbon nanotubes," *Composite Structures*, 88, 602 – 609, 2009.

[20] M. Rossi and M. Meo, "On the estimation of mechanical properties of single-walled carbon nanotubes by using a molecular-mechanics based fe approach," *Composites Science and Technology*, 69, 1394 – 1398, 2009.

[21] T. C. Theodosiou and D. A. Saravanos, "Molecular mechanics based finite element for carbon nanotube modeling," *ASME Conference Proceedings*, 2006, 55–64, 2006.

[22] J. R. Mianroodi and R. Naghdabadi, "Finite element implementation of embedded atomic potential for simulating particulate metal matrix nanocomposites," 3rd ECCOMAS thematic conference on the mechanical response of composites, 345–360, 2011.

[23] T. C. Theodosiou and D. A. Saravanos, "Numerical simulations using a molecular mechanics-based finite element approach: Application on boron-nitride armchair nanotubes," *International Journal for Computational Methods in Engineering Science and Mechanics*, 12, 203–211, 2011.

[24] L. Nasdala, A. Kempe, and R. Rolfes, "The molecular dynamic finite element method (mdfem)," *CMC*, 19, 57–104, 2010.

[25] B. Liu, Y. Huang, H. Jiang, S. Qu, and K. Hwang, "The atomic-scale finite element method," *Computer Methods in Applied Mechanics and Engineering*, 193, 1849 – 1864, 2004.

[26] G. Overney, W. Zhong, and D. Tomnek, "Structural rigidity and low frequency vibrational modes of long carbon tubules," *Zeitschrift für Physik D Atoms, Molecules and Clusters*, 27, 93–96, 1993.

[27] S. Govindjee and J. L. Sackman, "On the use of continuum mechanics to estimate the properties of nanotubes," *Solid State Communications*, 110, 227 – 230, 1999.

[28] D. Qian, G. J. Wagner, W. K. Liu, M.-F. Yu, and R. S. Ruoff, "Mechanics of carbon nanotubes," *Applied Mechanics Reviews*, 55, 495–533, 2002.

[29] L. Nasdala, A. Kempe, and R. Rolfes, "Are finite elements appropriate for use in molecular dynamic simulations?," *Composites Science and Technology*, 2012.

[30] J. Wackerfuß, "Molecular mechanics in the context of the finite element method," *International Journal for Numerical Methods in Engineering*, 77, 969–997, 2009.

[31] F. Scarpa, S. Adhikari, and A. S. Phani, "Effective elastic mechanical properties of single layer graphene sheets," *Nanotechnology*, 20, 065709, 2009.

[32] S. Sihn, V. Varshney, A. K. Roy, and B. L. Farmer, "Prediction of 3d elastic moduli and poissons ratios of pillared graphene nanostructures," *Carbon*, 50, 603 – 611, 2012.

[33] T. Belytschko, S. P. Xiao, G. C. Schatz, and R. S. Ruoff, "Atomistic simulations of nanotube fracture," *Phys. Rev. B*, 65, 235430, Jun 2002.

[34] C. Lobo and J. L. Martins, "Valence force field model for graphene and fullerenes," *Zeitschrift fr Physik D Atoms, Molecules and Clusters*, 159–164, 1997. 10.1007/s004600050123.

[35] A. Rappé and C. Casewit, *Molecular Mechanics Across Chemistry*. University Science Books, 1997.

[36] MathWorks, *MATLAB R2011b*. The MathWorks Inc., 3 Apple Hill Drive, Natick, MA 01760-2098, USA, 2011.

[37] Simulia, *ABAQUS 6.10-1*. Dassault Systemes Simulia Corp, Rising Sun Mills, 166 Valley Street, Providence, RI 02909-2499, USA, 2010.

[38] M. Dresselhaus, G. Dresselhaus, and R. Saito, "Physics of carbon nanotubes," *Carbon*, 33, 883 – 891, 1995.

[39] H. Terrones and A. Mackay, "The geometry of hypothetical curved graphite structures," *Carbon*, 30, 1251 – 1260, 1992.

[40] D. Baowan, B. J. Cox, and J. M. Hill, "Junctions between a boron nitride nanotube and a boron nitride sheet," *Nanotechnology*, 19, 075704, 2008.

[41] B. J. Cox and J. M. Hill, "A variational approach to the perpendicular joining of nanotubes to plane sheets," *Journal of Physics A: Mathematical and Theoretical*, 41, 125203, 2008.

[42] D. Baowan, B. Cox, and J. Hill, "Joining a carbon nanotube and a graphene sheet," in *Nanoscience and Nanotechnology, 2008. ICONN 2008. International Conference on*, 5 –8, feb. 2008.

[43] D. Baowan, B. J. Cox, and J. M. Hill, "Two least squares analyses of bond lengths and bond angles for the joining of carbon nanotubes to graphenes," *Carbon*, 45, 2972 – 2980, 2007.

[44] H. Terrones, "Curved graphite and its mathematical transformations," *Journal of Mathematical Chemistry*, 15, 143–156, 1994.

[45] A. L. Mackay, H. Terrones, and P. W. Fowler, "Hypothetical graphite structures with negative gaussian curvature [and discussion]," *Philosophical Transactions of the Royal Society of London. Series A: Physical and Engineering Sciences*, 343, 113–127, 1993.